Molecular Cancer Research

STEAP1 Is Associated with the Invasive and Oxidative Stress Phenotype of Ewing Tumors

Thomas G.P. Grunewald[1,3], Isabel Diebold[4], Irene Esposito[2,5], Stephanie Plehm[1], Kristina Hauer[1], Uwe Thiel[1], Patricia da Silva-Buttkus[5], Frauke Neff[5], Rebekka Unland[7,8], Carsten Müller-Tidow[7], Colette Zobywalski[1], Katharina Lohrig[9], Urs Lewandrowski[9], Albert Sickmann[9,10], Olivia Prazeres da Costa[6], Agnes Görlach[4], Andrea Cossarizza[11], Elke Butt[12], Günther H.S. Richter[1], and Stefan Burdach[1]

Abstract

Ewing tumors comprise the second most common type of bone-associated cancer in children and are characterized by oncogenic EWS/FLI1 fusion proteins and early metastasis. Compelling evidence suggests that elevated levels of intracellular oxidative stress contribute to enhanced aggressiveness of numerous cancers, possibly including Ewing tumors. Using comprehensive microarray analyses and RNA interference, we identified the six-transmembrane epithelial antigen of the prostate 1 (STEAP1)—a membrane-bound mesenchymal stem cell marker of unknown function—as a highly expressed protein in Ewing tumors compared with benign tissues and show its regulation by EWS/FLI1. In addition, we show that STEAP1 knockdown reduces Ewing tumor proliferation, anchorage-independent colony formation as well as invasion *in vitro* and decreases growth and metastasis of Ewing tumor xenografts *in vivo*. Moreover, transcriptome and proteome analyses as well as functional studies revealed that STEAP1 expression correlates with oxidative stress responses and elevated levels of reactive oxygen species that in turn are able to regulate redox-sensitive and proinvasive genes. In synopsis, our data suggest that STEAP1 is associated with the invasive behavior and oxidative stress phenotype of Ewing tumors and point to a hitherto unanticipated oncogenic function of STEAP1. *Mol Cancer Res; 10(1); 52–65. ©2011 AACR.*

Introduction

Ewing tumors are highly metastatic bone-associated cancers of enigmatic histogenesis mostly affecting children. Established therapies still have limited success in advanced stages of the disease despite high toxicity (1). Thus, selective and less toxic drugs are the prerequisites to reduce the toxic burden of cure.

Ewing tumors express chimeric EWS/ETS (Ewing sarcoma breakpoint region 1/E-twenty-six) fusion proteins derived from chromosomal translocations with EWS/FLI1 (Ewing sarcoma breakpoint region 1/friend leukemia virus integration 1) being the predominant one (85%). *EWS/FLI1* encodes an oncogenic transcription factor that determines the complex and highly malignant phenotype of Ewing tumors (2). Hence, the detailed functional characterization of the EWS/FLI1-induced transcriptome may be key to understand the underlying mechanisms of the disease and ultimately to halt its progression (3, 4).

Previously, we identified a specific expression signature of approximately 40 genes that are highly upregulated in Ewing tumors compared with benign tissues (3). Part of this signature is the six-transmembrane epithelial antigen of the prostate 1 (STEAP1)—a membrane-bound protein possibly contributing to transmembrane electron transfer (5, 6).

Among STEAP proteins, only STEAP1 is overexpressed in many carcinomas including prostate and bladder cancer, where it locates to plasma and endosomal membranes (6, 7), but its precise cellular function remains elusive. Recently, STEAP1 was validated as a bona fide marker for mesenchymal stem cells (MSC; ref. 8) supporting the relationship of Ewing tumors with MSCs (9). Moreover, STEAP1 mRNA

Authors' Affiliations: [1]Children's Cancer Research and Roman Herzog Comprehensive Cancer Center, Laboratory of Functional Genomics and Transplantation Biology, [2]Institute of Pathology, Klinikum rechts der Isar; [3]Medical Life Science and Technology Center; [4]Experimental and Molecular Pediatric Cardiology, German Heart Center Munich; [5]Institute of Pathology, Helmholtz-Zentrum München; [6]Institute for Medical Microbiology, Immunology and Hygiene, Institute of Advanced Study, Technische Universität München, München; [7]Department of Medicine, Hematology, and Oncology, and Interdisciplinary Center for Clinical Research (IZKF), University of Münster; [8]Department of Pediatric Hematology and Oncology, University Children's Hospital Münster, Münster; [9]Leibniz–Institut für Analytische Wissenschaften–ISAS e.V., Dortmund; [10]Medical Proteome Center (MPC), Ruhr-University Bochum, Bochum, Germany; [11]Department of Biomedical Sciences, University of Modena and Reggio Emilia School of Medicine, Italy; and [12]Institute for Clinical Biochemistry, University of Würzburg, Würzburg, Germany

Note: Supplementary data for this article are available at Molecular Cancer Research Online (http://mcr.aacrjournals.org/).

G.H.S. Richter and S. Burdach share senior authorship.

Corresponding Author: Thomas G.P. Grunewald, Technische Universität München, Kölner Platz 1, Munich 80804, Germany. Phone: 4989-3068-5525; Fax: 4989-3068-3791; E-mail: thomas.gruenewald@lrz.tum.de

doi: 10.1158/1541-7786.MCR-11-0524

circulates in peripheral blood (6, 10), and its detection in bone marrow of patients with Ewing tumors is indicative for occult Ewing tumor cells (11).

In contrast, STEAP1 mRNA is not detectable in blood of healthy donors and is hardly expressed in benign tissues, except for low amounts in urothelium and prostate (6, 10). Because of its high tumor specificity and membrane-bound localization, STEAP1 might serve as a promising candidate for targeted therapy (6, 10, 11). In accordance, monoclonal antibodies against STEAP1 inhibit growth of xenografted prostate and bladder cancer (12).

STEAP proteins are homologues of NADPH oxidases (NOX; refs. 13, 14), which are involved in cellular reactive oxygen species (ROS) metabolism and frequently overexpressed in cancer (15). Like NOX, all STEAP proteins, except for STEAP1, are equipped with an N-terminal $NADP^+$ oxidoreductase (7, 13). In addition, all STEAP members contain a C-terminal ferric oxidoreductase. Thus, a role in cellular iron homeostasis is assumed for these proteins (16). However, in contrast to other STEAP proteins, STEAP1 does not facilitate iron uptake and reduction, suggesting another distinct function (7).

ROS play a key role in oncogenic signaling and elevated ROS levels are a salient feature of many highly invasive cancers (17, 18), possibly including Ewing tumors (19). Sound evidence suggests that many malignancies take advantage of a permanently active "oxidative stress phenotype" leading to enhanced invasiveness, which has been recognized as an additional hallmark of cancer (20). On the basis of its homology to NOX and its overexpression in highly metastatic cancers, we hypothesized that STEAP1 is involved in the invasive behavior and oxidative stress phenotype of Ewing tumors.

In the present study, we investigate the putative oncogenic function of STEAP1. We prove that *STEAP1* is induced by EWS/FLI1 and that its expression promotes proliferation, invasiveness, anchorage-independent colony formation, tumorigenicity, and metastasis of Ewing tumors. Moreover, transcriptome and proteome analyses as well as functional studies reveal that STEAP1 expression is associated with elevated ROS levels that regulate ROS-sensitive signaling molecules and proinvasive genes via STAT1.

Materials and Methods

Cell lines and reagents

Ewing tumor cell lines (MHH-ES1, SK-ES1, RDES, SK-N-MC, TC-71), neuroblastoma lines (CHP126, MHH-NB11, SHSY5Y, SIMA), rhabdomyosarcoma cell line RH-30, and B-cell leukemia lines (Nalm6, 697, cALL2) were obtained from the German Collection of Microorganisms and Cell Cultures (DSMZ). A673 was purchased from American Type Culture Collection (LGC Standards). SB-KMS-KS1, previously described as SBSR-AKS, is an Ewing tumor cell line with a type 1 *EWS/FLI1* translocation established in our laboratory (4). Human MSCs L87 and V54.2 were immortalized with SV40 large T-antigen (4). Retrovirus packaging cell line PT67 was obtained from Takara Bio Europe/Clontech. Cells were grown at 37°C in 5% CO_2 in a humidified atmosphere in RPMI-1640 (Invitrogen) containing 10% FBS (Biochrom), 1% glutamine, and 100 μg/mL gentamycin (Invitrogen). Cell lines were checked routinely for purity (EWS/FLI1 translocation product, surface antigen, or HLA-phenotype) and Mycoplasma contamination. Reagents were purchased from Sigma, if not otherwise specified.

Quantitative real-time PCR

Gene expression was analyzed using TaqMan Universal PCR Master Mix, TaqMan Gene Expression Assays, and fluorescence detection with an AB 7300 Real-Time PCR System (Applied Biosystems). Results were normalized to glyceraldehyde-3-phosphate dehydrogenase (GAPDH) and quantified by the $\Delta\Delta C_t$ method. Primers are listed in Supplementary Methods.

RNA interference

Transfection was described previously (4). For siRNA, see Supplementary Methods.

Chromatin immunoprecipitation

Chromatin immunoprecipitation was essentially carried out as described (4). For primers, see Supplementary Methods.

Western blotting

Procedures were described previously (4). For antibodies, see Supplementary Methods. Specificity of the STEAP1 antibody was assessed previously (21, 22).

Tissue samples

The Institutional Review Board of the Technische Universität München (Munich, Germany) approved the current study. Archival tumor samples were obtained from the Department of Pathology of the Technische Universität München.

Histology and immunohistochemistry

Procedures were described previously (4). See Supplementary Methods.

Microarrays

Experiments were essentially carried out as described previously (4). See Supplementary Methods.

Two-dimensional gel electrophoresis and mass spectrometry

Two-dimensional (2D) isoelectric focusing/SDS-PAGE were essentially carried out as described previously (23). For spot selection and mass spectrometry, see Supplementary Methods.

Flow cytometry

Cells were stained 48 to 72 hours after transfection as described (24). Samples were analyzed on a FACScalibur

flow cytometer (Becton Dickinson). At least 30,000 events per sample were recorded. See Supplementary Methods.

Proliferation assays

Cell numbers were counted in real-time with a bioelectric xCELLigence instrument (Roche/ACEA Biosciences) monitoring impedance across gold micro-electrodes on the bottom of E-plates. Immediately after transfection with siRNA, 1.6×10^4 cells were seeded in wells in 200 μL media containing 10% FBS. Cellular impedance was measured periodically. Transfection efficacy was controlled by Western blot analysis and/or quantitative real-time PCR (qRT-PCR).

Invasion assays

A total of 5×10^5 transiently transfected cells in 500 μL serum-free media was seeded into the upper chambers of Matrigel-covered Transwell plates (Becton Dickinson). Bottom chambers contained 500 μL media with 10% FBS. After 48 hours, invading cells were stained with 4 μg/mL CalceinAM (Becton Dickinson) in Hank's balanced salt solution and photographed with a Zeiss AxioCam MRm camera on a Zeiss Axiovert 100 microscope (Zeiss). The number of invading cells was normalized to proliferation as assessed with xCELLigence (Roche/ACEA Biosciences). *N*-Acetylcysteine (NAC) or H_2O_2 pretreatment of Matrigel plates did not affect invasiveness of untreated Ewing tumor cells plated subsequently.

Constructs and retroviral gene transfer

See Supplementary Methods.

Colony-forming assay

Procedures were described previously (4).

Mice and *in vivo* experiments

Immunodeficient $Rag2^{-/-}\gamma_c^{-/-}$ mice on a BALB/c background were obtained from the Central Institute for Experimental Animals (Kawasaki) and maintained under pathogen-free conditions in accordance with the institutional guidelines and approval by local authorities. Experiments were carried out in 6- to 16-week-old mice. For *in vivo* tumor growth, 3×10^6 Ewing tumor cells in 0.2 mL PBS were subcutaneously injected in groins. The amount of 2×10^6 to 5×10^6 cells has been previously reported to be optimal for assessment of local growth of Ewing tumor xenografts (4, 25). Mice bearing tumors greater than 10 mm in diameter (determined with a caliper) were considered positive (event). To analyze metastatic potential, tumor cells were injected intravenously. Five weeks later, mice were euthanized and metastasis was monitored in individual organs. All macroscopically visible metastases within an organ were counted. Tumors and affected tissues were excised for histology and gene expression analysis.

Measurement of ROS and mitochondrial mass

Procedures were described previously (26). See Supplementary Methods.

Glutathione assay

Cellular glutathione was assessed with a colorimetric assay kit following the manufacturer's instructions (Cayman Europe).

Electron microscopy

Procedures were described previously (27, 28).

Statistics

Unpaired two-tailed Student *t* test or independent one-sample *t* test were used; $P < 0.05$ was considered significant.

Results

STEAP1 is highly expressed in Ewing tumors and induced by EWS/FLI1

Previously, we identified STEAP1 in an Ewing tumor expression signature (3). To substantiate this observation, we matched our microarray data against those of neuroblastomas and a normal body map composed of benign fetal and adult tissues. As seen in Fig. 1A and B, STEAP1 is highly expressed in Ewing tumors but virtually not expressed in neuroblastomas and benign tissues. High STEAP1 expression in Ewing tumors was confirmed by qRT-PCR and Western blot analysis (Fig. 1C). To test whether EWS/ETS transcription factors can induce STEAP1, we transfected MSCs with *EWS/FLI1*-containing vectors and observed a 5- to 6-fold increase of STEAP1 expression in 2 MSC lines (L87 and V54.2; Fig. 1D). Vice versa, RNA interference–mediated EWS/FLI1 silencing in Ewing tumor cells reduced STEAP1 expression (Fig. 1E). Moreover, the *STEAP1* promoter contains 2 evolutionarily conserved ETS-binding sites (−1,465 and −250 bp upstream of the transcriptional start site), which proved to be enriched for FLI1 in chromatin immunoprecipitation (Fig. 1F). We next confirmed STEAP1 overexpression in primary Ewing tumors on protein level. As positive controls, we chose prostate cancer because of its known overexpression of STEAP1 (6). Figure 1G shows that among a series of tumors, which are usually included in the histologic differential diagnosis of Ewing tumors (29, 30), only Ewing tumors display very high STEAP1 levels. Consistently, the analysis of a sarcoma gene expression library (137 sarcomas; 14 entities) revealed that STEAP1 discriminates Ewing tumors from other sarcomas (sensitivity, 89.5%; specificity, 82.2%; ref. 31).

Knockdown of STEAP1 inhibits proliferation, invasion, anchorage-independent colony formation, tumorigenicity and metastasis of Ewing tumor cells

Because STEAP1 is overexpressed in Ewing tumors, we tested whether RNA interference–mediated STEAP1 silencing impacts the Ewing tumor phenotype. Using an xCELLigence instrument, we observed that STEAP1 knockdown reduced proliferation of Ewing tumor cells (Fig. 2A) without affecting rates of apoptosis and/or necrosis or inducing cell-cycle arrest (Supplementary Fig. S1). Moreover, STEAP1 silencing inhibited cellular invasiveness through Matrigel (Fig. 2B), whereas STEAP1 overexpression in Ewing tumor

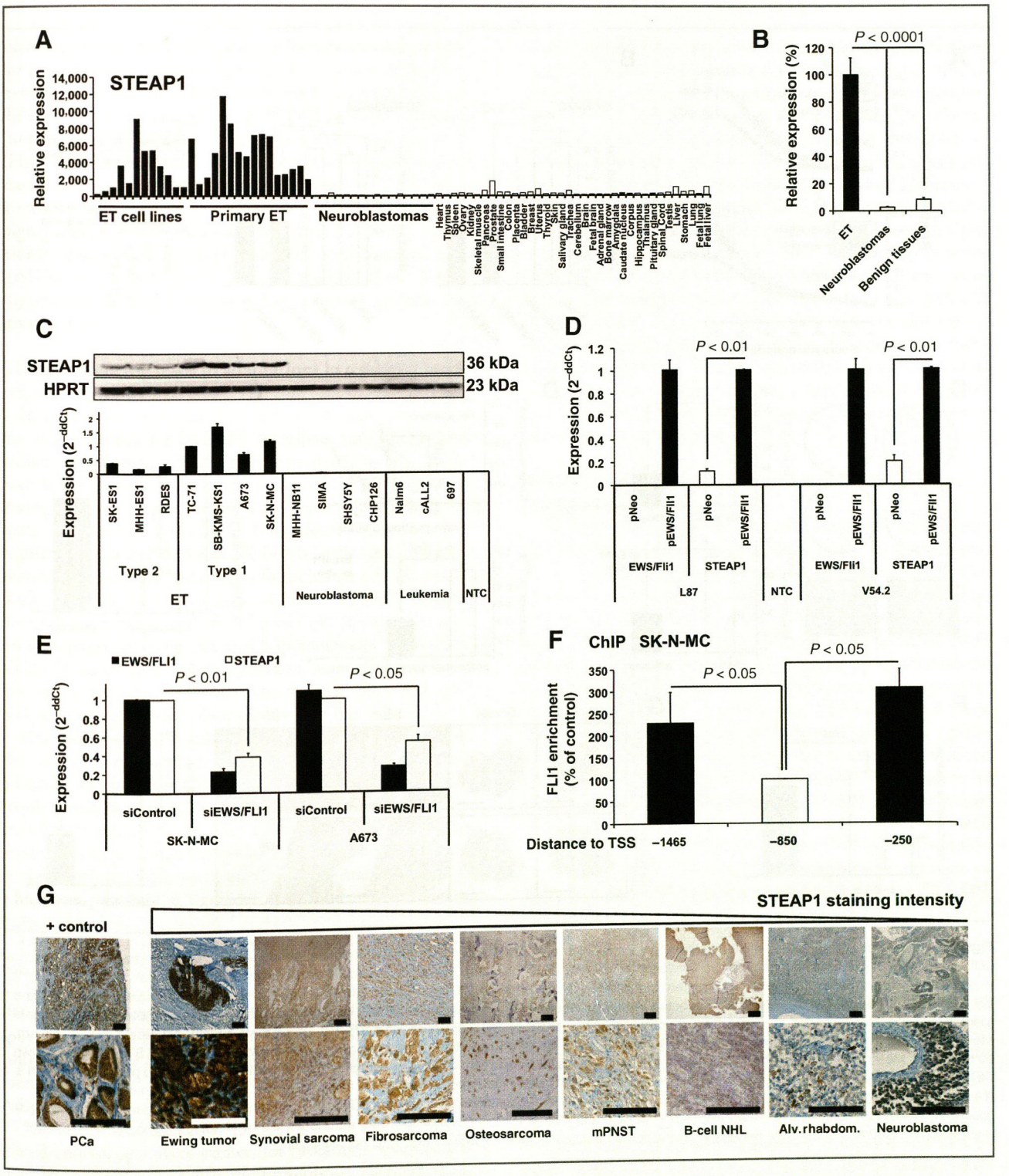

Figure 1. STEAP1 is highly expressed in Ewing tumors (ET) and induced by EWS/FLI1. A and B, RNA microarrays of 26 Ewing tumors and 16 neuroblastomas (GSE1824, GSE1825, GSE15757) compared with 36 benign tissues (GSE2361) for STEAP1 expression. Mean ± SEM. C, quantification of STEAP1 by qRT-PCR and Western blot analysis in Ewing tumor (type 1 and 2 translocation), neuroblastoma, and leukemia cell lines. Mean ± SEM of 3 experiments (duplicates/group). Loading control: hypoxanthine phosphoribosyltransferase 1 (HPRT); NTC, no template control. D, analysis of STEAP1 and EWS/FLI1 by qRT-PCR in MSCs (L87 and V54.2) transfected with pMSCVews/fli1 (pEWS/FLI1) or empty vector (pNEO). Mean ± SEM of 3 experiments/cell line (duplicates/group). E, expression of STEAP1 and EWS/FLI1 in Ewing tumor cell lines after EWS/FLI1 silencing. Mean ± SEM of 2 experiments/cell line (duplicates/group). F, chromatin immunoprecipitation (ChIP) of the *STEAP1* promoter: FLI1 is enriched at the ETS consensus sites at −250 and −1,465 bp upstream of the transcriptional start site (TSS). The −850-bp region is devoid of the ETS recognition sequences and served as negative control. Mean ± SEM of 3 ChIPs; *t* test. G, immunohistochemistry for STEAP1 of prostate cancer (PCa), Ewing tumor, synovial sarcoma, sclerosing epithelioid fibrosarcoma, osteosarcoma, malignant peripheral nerve sheath tumor (mPNST), B-cell non–Hodgkin lymphoma (NHL), alveolar rhabdomyosarcoma (Alv. rhabdom), and neuroblastoma. Scale bars, 500 and 125 μm.

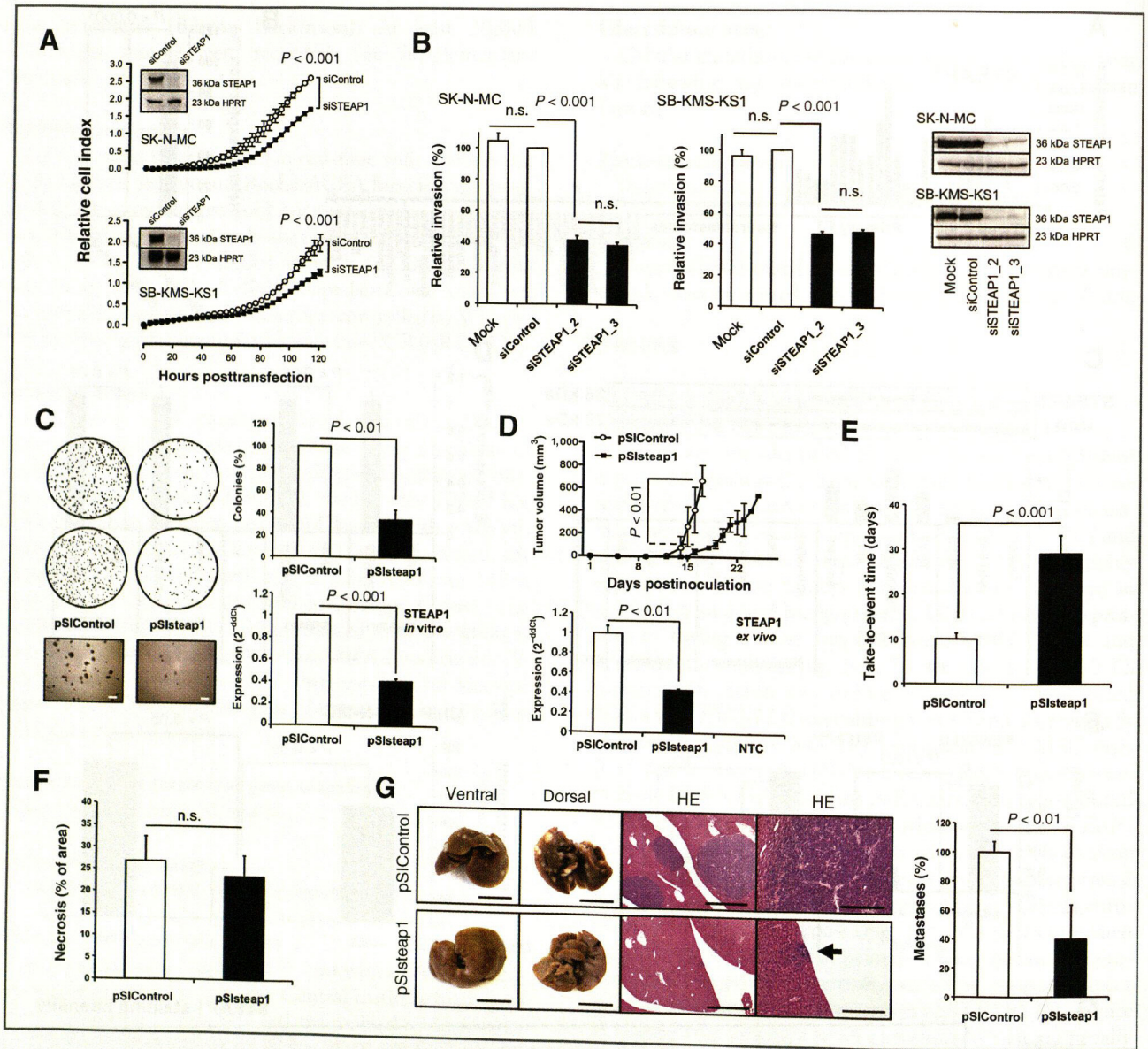

Figure 2. Knockdown of STEAP1 inhibits proliferation, invasion, anchorage-independent colony formation, tumorigenicity, and metastasis of Ewing tumor cells. A, analysis of proliferation of transfected Ewing tumor cells with xCELLigence. Cellular impedance is displayed as relative cell index. Mean ± SEM of 2 experiments/cell line (heptaplicates/group). Western blot analysis was conducted 100 hours after transfection. B, analysis of invasiveness of SK-N-MC and SB-KMS-KS1 (transfected with siRNA 48 hours before seeding). Western blot analyses show STEAP1 knockdown efficacy. Mean ± SEM of 3 experiments (pentaplicates/group). C, anchorage-independent colony formation of SK-N-MC with constitutive STEAP1 knockdown (pSIsteap1). Scale bars, 1,000 μm. Mean ± SEM of 3 experiments (duplicates/group). D, tumorigenicity of SK-N-MC infectants (5 mice per group) and *ex vivo* confirmation of STEAP1 knockdown by qRT-PCR. Mean ± SEM. E, combined analysis of tumor growth as take-to-event time of 3 experiments (14 mice pSIControl; 18 mice pSIsteap1). Mean ± SEM. "Take" is the day when the tumor exceeded 2 mm and "event" when the tumor exceeded 10 mm in diameter. F, quantification of necrotic area (14 xenografts per group). Mean ± SEM of 3 experiments. G, evaluation of metastatic potential of pSIsteap1 infectants (intravenously injected; 4 mice per group). All macroscopically visible metastases were counted and their small round blue phenotype was confirmed by histology (scale bar = 10 mm for macroscopy, 1,000 and 100 μm for histology; arrow, micrometastasis). Mean ± SEM; *t* test. n.s., nonsignificant.

cells with low STEAP1 expression increased invasiveness and proliferation (Supplementary Fig. S1). Interestingly, STEAP1 levels correlated with invasiveness of different Ewing tumor cell lines (Supplementary Fig. S1). To evaluate the effect of long-term knockdown of STEAP1, we generated STEAP1 short hairpin RNA–expressing infectants of 2 Ewing tumor cell lines (SK-N-MC and SB-KMS-KS1). Constitutive STEAP1 silencing reduced colony formation of Ewing tumor cells in methylcellulose in a dose-dependent manner (Fig. 2C and Supplementary Table S1). Consistently, these infectants exhibited delayed tumor growth in $Rag2^{-/-}\gamma_c^{-/-}$ mice (Fig. 2D and E). Persistence of STEAP1 knockdown was confirmed *ex vivo* in each xenograft (Fig. 2D). Comparing the xenografts with or without STEAP1

silencing, we did not find changes in immunohistochemistry for the apoptosis marker caspase-3 or for tumor-infiltrating macrophages (tested by MAC3; not shown). In addition, no differences in vascularization, quantified by CD31 staining (not shown), and in intratumoral necrosis were observed (Fig. 2F). Similarly to local tumor growth, experimental metastasis into the liver was diminished after STEAP1 knockdown (Fig. 2G). Although our cell lines showed a high propensity to metastasize into livers, we only noted kidney metastases in mice injected with control cells (pSIControl; not shown). Taken together, these results suggest that STEAP1 supports Ewing tumor growth and invasiveness.

STEAP1 silencing leads to adaptations in oxidative stress response systems

In accordance with data in HEK-293T cells (7), we did not find evidence for STEAP1 to impact iron uptake and reduction in Ewing tumors (Supplementary Fig. S2). However, to gain functional insight into how STEAP1 influences Ewing tumor malignancy, we conducted whole transcriptome microarrays (GSE26422) to identify concordantly regulated genes in A673 and SK-N-MC cells after STEAP1 silencing (minimum mean $\log_2$ fold change ± 0.32; maximum variation of 40% across siRNAs). STEAP1 knockdown differentially regulates 87 genes (41 upregulated and 46 downregulated; Fig. 3A and Supplementary Table S2). STEAP1-dependent gene regulation was confirmed on selected genes after STEAP1 knockdown (Fig. 3B) and STEAP1 overexpression (Supplementary Fig. S2).

Among the 40 top-regulated genes, 20% were assigned to the ubiquitin–proteasome system (UPS), suggesting that STEAP1 might play a role in protein modification that requires enhanced proteasomal decay. Consistently, gene set enrichment analysis (GSEA) revealed that STEAP1 silencing regulates gene sets involved in oxidative stress responses, type II conjugation, and proteolysis (Supplementary Table S3), which are part of the oxidative stress phenotype seen in cancer (32, 33).

In support of the prediction that changes in oxidative stress responses influence overall proteome composition, STEAP1 knockdown altered the protein levels of 121 spots (81 spots upregulated and 40 spots downregulated) of 845 spots detected in 2D gel electrophoresis of SK-N-MC cells (minimum linear fold change ± 2 in 3 independent experiments as assessed by densitometric analysis with PDquest Advanced; BioRad; $P < 0.05$).

The 24 most significantly regulated spots and 1 nonregulated control spot were excised for proteomic analysis. By mass spectrometry, 132 different proteins were identified, of which 17% were assigned to protein transport and folding, 13% to invasion, and 11% to the redox system according to their gene ontology (GO) annotations (Fig. 3C). Among these proteins are several redox enzymes such as peroxiredoxins and superoxide dismutases, which are dysregulated in a large cohort of cancers (15, 34). Moreover, endosomal redox stress response proteins (35, 36) were identified including T-complex chaperones, heat shock proteins, protein-disulfide isomerases as well as co-chaperones. Furthermore, we identified mediators of posttranscriptional mRNA processing such as heterogeneous nuclear ribonucleoproteins, THO complex proteins, and eukaryotic translation initiation factors (Supplementary Table S4). Notably, we found dysregulation of 2 of 6 key modules of the hexameric proteasomal ATPase (PSMC5 and PSMC6) and identified 2 further subunits (PSMC3 and PSMC4) in regulated spots by proteomic means as well as key modules of the proteolytic cavities of the proteasome and immunoproteasome (PSMA3, PSMB5, PSMB8, and PSMB9), which are critical for protein quality control upon oxidative stress (ref. 37; Supplementary Fig. S2). These data were confirmed by GSEA pathway analysis (Table 1). In summary, these analyses suggest that STEAP1 silencing leads to adaptations in oxidative stress response systems, supporting the hypothesis that STEAP1 is associated with the oxidative stress phenotype of Ewing tumors.

STEAP1 expression is associated with ROS levels of Ewing tumors cells

We next investigated whether the long-term knockdown of STEAP1 can lead to altered ROS levels. Indeed, constitutive STEAP1 silencing decreased ROS-levels (Fig. 4A), whereas STEAP1 overexpression increased ROS levels (Fig. 4B) as quantified by dihydroethidium fluorescence. Moreover, STEAP1 knockdown reduced mitochondrial ROS without changing mitochondrial mass as quantified by MitoSOX Red and MitoTracker Green staining, respectively (Fig. 4C and D). Consistently, STEAP1 knockdown decreased the cellular pool of oxidized glutathione (glutathione disulfide) but increased the amount of reduced glutathione (GSH; Fig. 4E). Interestingly, reassessment of our microarray data revealed that STEAP1 is most prominently expressed in Ewing tumors among other NOX and STEAP proteins (Supplementary Fig. S3). It should be noted that we did not detect obvious morphologic changes of Ewing tumor cells and their mitochondria upon STEAP1 knockdown (Fig. 4F).

ROS are critical for Ewing tumor proliferation and invasiveness

Our data and recent discussion in the literature (19) indicate that ROS might promote Ewing tumor aggressiveness. In accordance, treatment of Ewing tumor cells with the antioxidant NAC reduced colony formation, proliferation, and invasiveness of Ewing tumor cells in a dose-dependent manner (Fig. 5A–C). Similar results have been obtained with PEGylated-superoxide dismutase and PEGylated-catalase (Supplementary Fig. S4). Reciprocally, treatment of STEAP1 silenced Ewing tumor cells with H_2O_2 rescued the invasive phenotype of STEAP1 knockdown cells (Fig. 5D).

We next tested whether STEAP1-regulated genes contribute to the oxidative stress phenotype observed. We choose MMP-1, ADIPOR1, and DTX3L for follow-up due to their high expression in Ewing tumors and their involvement in oxidative stress responses (34, 38, 39). Notably,

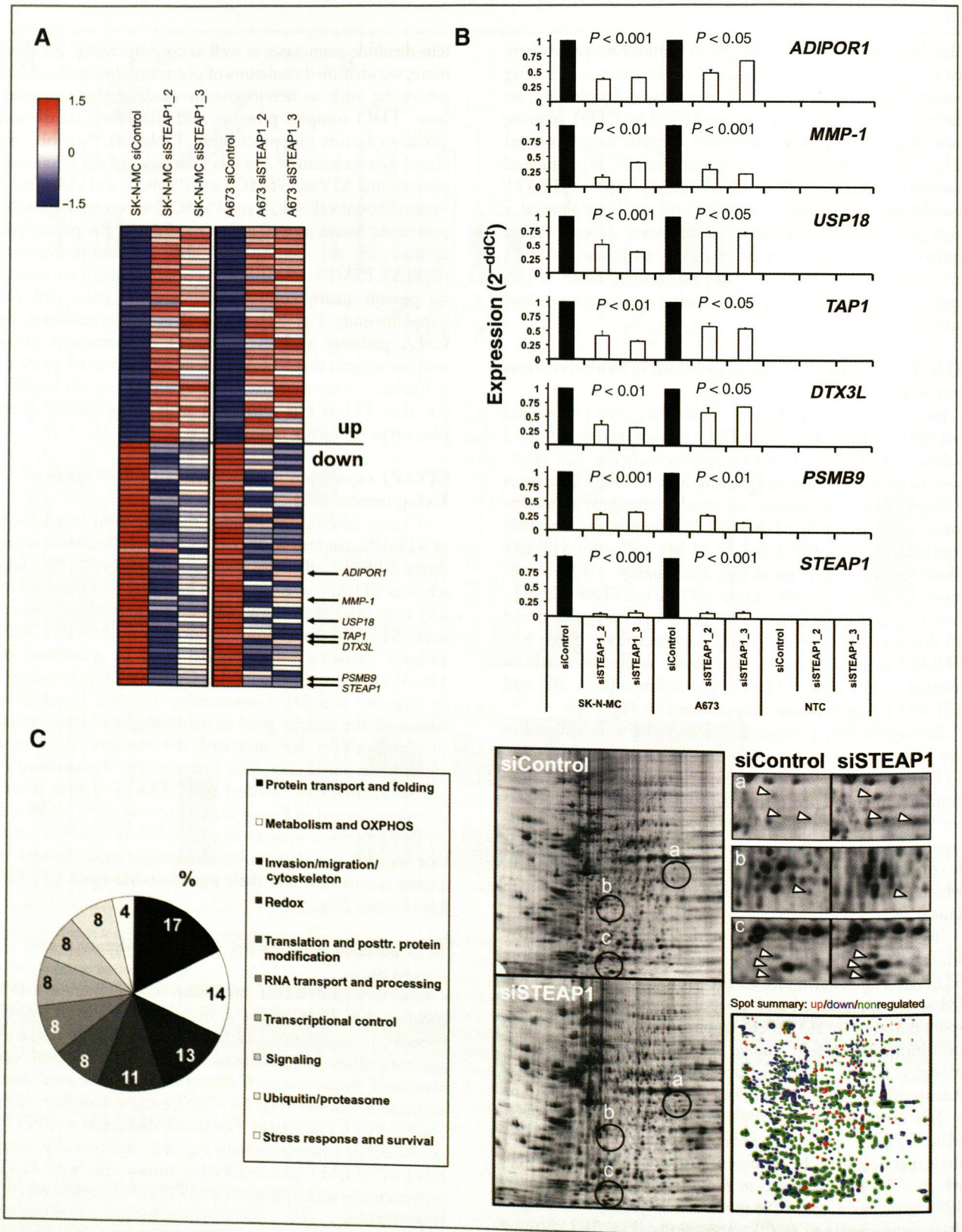

Figure 3. STEAP1 silencing leads to adaptations in oxidative stress response systems. A, heatmaps of differentially expressed genes after STEAP1 silencing (normalized median centered $\log_2$ values) including genes selected for validation (arrows). B, validation of differential gene expression by qRT-PCR. ADIPOR1, adiponectin receptor 1; MMP-1, matrix metallopeptidase 1; USP18, ubiquitin-specific peptidase 18; TAP1, transporter 1, ATP-binding cassette, sub-family B; DTX3L, E3 ubiquitin–protein ligase deltex 3-like; PSMB9, proteasome subunit β-9. Mean ± SEM of at least 2 experiments/cell line (duplicates/group); *t* test. C, left, distribution of functional GO annotations of differentially expressed proteins in SK-N-MC as identified by 2D gel electrophoresis and mass spectrometry 72 hours after RNA interference. Right, representative 2D gels of siControl and siSTEAP1, micrographs showing regulated spots (arrows), and the computational overlay summary of up, down, and nonregulated spots of 3 experiments.

Table 1. GSEA pathway analysis of differentially regulated proteins as identified by 2D gel electrophoresis and mass spectrometry

Gene set name[a]	Function	K[b]	k[c]	k/K	P
REACTOME_CHAPERONIN_MEDIATED_PROTEIN_FOLDING	Chaperonin-mediated protein folding	50	7	0.14	<0.001
REACTOME_PREFOLDIN_MEDIATED_TRANSFER_OF_SUBSTRATE_TO_CCT_TRIC	Chaperonin-mediated protein folding	28	7	0.25	<0.001
REACTOME_FORMATION_OF_TUBULIN_FOLDING_INTERMEDIATES_BY_CCT_TRIC	Chaperonin-mediated protein folding	22	6	0.27	<0.001
KEGG_PROTEASOME	Proteasomal protein decay	48	6	0.13	<0.001
REACTOME_SCF_BETA_TRCP_MEDIATED_DEGRADATION_OF_EMI1	Ubiquitin ligase–mediated protein processing	48	6	0.13	<0.001
REACTOME_SCF_SKP2_MEDIATED_DEGRADATION_OF_P27_P21	Ubiquitin ligase–mediated protein processing	52	6	0.12	<0.001
REACTOME_ASSOCIATION_OF_TRIC_CCT_WITH_TARGET_PROTEINS_DURING_BIOSYNTHESIS	Chaperonin-mediated protein folding	29	5	0.17	<0.001
REACTOME_METABOLISM_OF_PROTEINS	Translation, posttranslational modification, and protein folding	215	12	0.06	0.024

[a]REACTOME, BIOCARTA, and KEGG pathway gene sets were used for analysis.
[b]K = number of genes in gene set.
[c]k = number of genes in overlap.

expression of MMP-1, ADIPOR1, and DTX3L appeared to be ROS sensitive in Ewing tumor cells as H_2O_2 treatment induced their expression in a time-dependent manner (Fig. 5E). Moreover, H_2O_2 treatment rescued MMP-1, ADIPOR1, and DTX3L, but not STEAP1, expression in a dose-dependent manner implying that STEAP1 is upstream of ROS signaling whereas the other genes are potentially downstream (Fig. 5F). Interestingly, silencing of these genes reduced invasiveness through Matrigel (Fig. 5G), whereas only ADIPOR1 knockdown significantly reduced Ewing tumor proliferation (Fig. 5H). In summary, these data suggest that oxidative stress may support Ewing tumor aggressiveness possibly, in part, via enhanced expression of MMP-1, ADIPOR1, and DTX3L.

STEAP1 knockdown inhibits STAT1 activation

Using GSEA to search for common transcription factor motifs within the 87 differentially regulated genes after STEAP1 silencing, we identified STAT1 ($P = 0.07$) and its downstream cofactors, IFN response factors (IRF) 1, 2, 7, and 8 ($P < 0.05$; ref. 40) as top-ranked putative STEAP1 targets. Consistently, interrogation of the GSEA Molecular Signatures Database (C2; v3.0) with these 87 genes revealed a strong overrepresentation of gene sets involved in IFN signaling accompanying STEAP1 expression (Fig. 6A and B). Interestingly, STAT1, a downstream effector of ROS and IFNs (41), is predominantly expressed in Ewing tumors (Fig. 6C). Of note, alike STEAP1 silencing, STAT1 silencing reduced the expression of STEAP1 target genes but left STEAP1 expression unaffected. Moreover, the downregulation of these genes could (apart from MMP-1 in 2 of 3 cell lines tested) not be rescued by H_2O_2, suggesting that STAT1 may be downstream of ROS and STEAP1 (compare Figs. 6D and 5F). Indeed, STEAP1 silencing results in less phosphorylated STAT1, which can be rescued by exogenous H_2O_2 and IFN-γ (Fig. 6E). However, Ewing tumor cells virtually do not endogenously produce IFNs and STEAP1 silencing neither alters their expression nor their secretion as seen by microarray (Fig. 6F) and ELISPOT analyses (Supplementary Fig. S5). In summary, these data indicate that STEAP1 and ROS may, in part, mediate their transcriptional effects via IFN-independent activation of STAT1 (Fig. 6G).

Discussion

The current study assessed the involvement of STEAP1 in the invasive and oxidative stress phenotype of Ewing tumors. We show that *STEAP1* is induced by EWS/FLI1 and important for Ewing tumor malignancy. Moreover, our data support a model whereby STEAP1 expression is linked to the maintenance of oxidative stress of Ewing tumors and increased Ewing tumor aggressiveness, probably mediated via STAT1. We show that STEAP1 is highly expressed in Ewing tumors compared with benign tissues and a series of other sarcomas implying that STEAP1 could be used in routine pathology as an additional marker for Ewing tumor diagnosis.

Our data indicate that STEAP1 is important for anchorage-independent colony formation and invasiveness of Ewing tumor cells *in vitro* and for tumorigenicity and metastasis *in vivo*. Moreover, we show that STEAP1 expression correlates with increased cellular ROS levels, which in turn induce the redox-sensitive and proinvasive

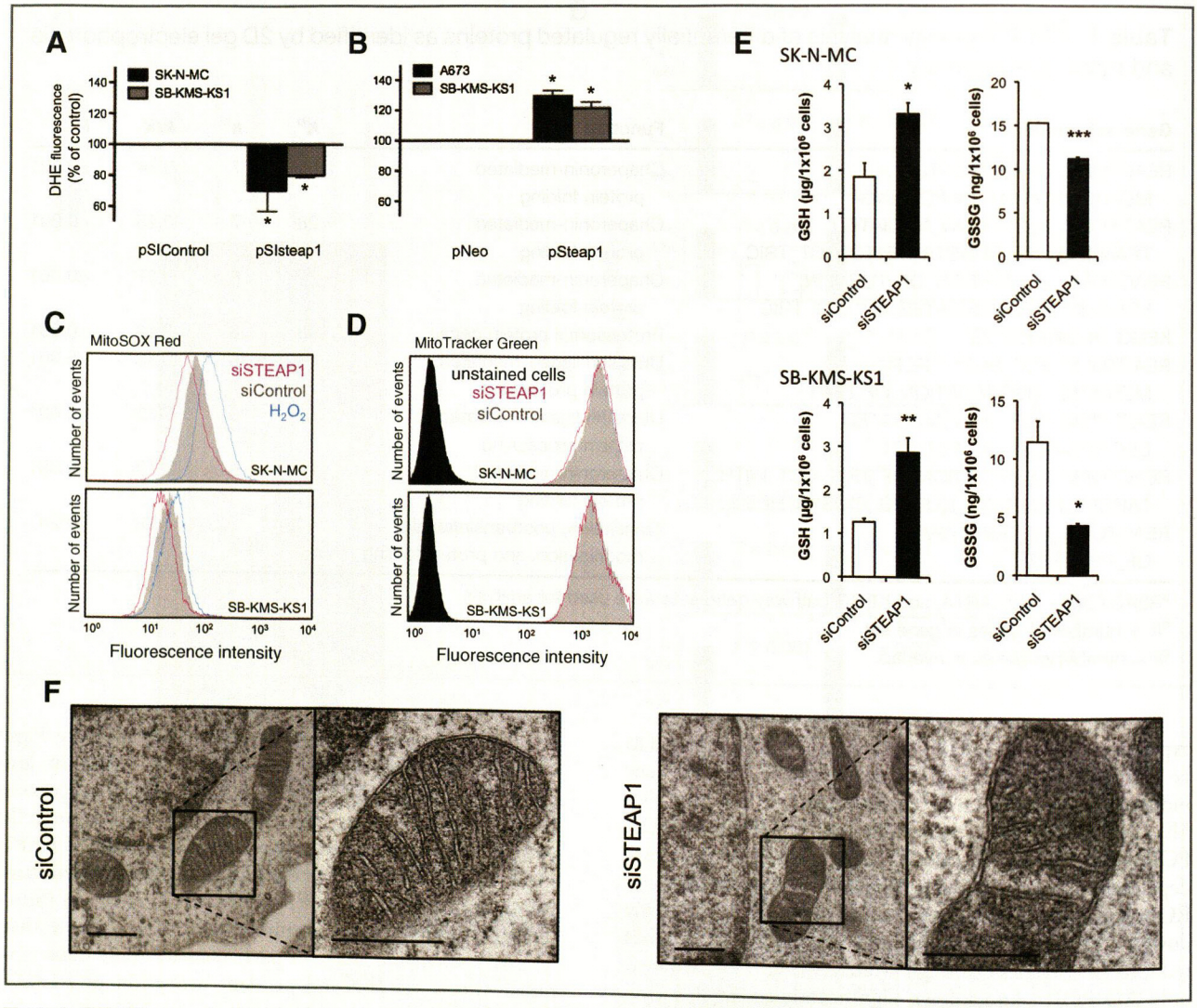

Figure 4. STEAP1 expression is associated with ROS levels of Ewing tumor cells. A and B, measurement of ROS with dihydroethidium (DHE) fluorescence after constitutive STEAP1 silencing (pSIsteap1) or STEAP1 overexpression (pSteap1). Mean ± SEM of 3 experiments/cell line (octaplicates/group). Controls set as 100%. C and D, representative images of flow cytometric measurements of mitochondrial ROS (MitoSOX Red) and mitochondrial mass (MitoTracker Green) in an aliquot of the cells was preincubated with 100 µmol/L hydrogen peroxide (H_2O_2; blue). E, analysis of reduced (GSH) and oxidized glutathione (glutathione disulfide; GSSG) 48 hours after transfection. Mean ± SEM of 2 experiments/cell line. F, low-power electron micrographs of SK-N-MC 80 hours after transfection showing no differences in mitochondrial morphology (scale bars, 0.4 µm). *, $P < 0.05$; **, $P < 0.01$; ***, $P < 0.001$; *t* test.

genes *MMP-1*, *DTX3L*, and *ADIPOR1*. Consistently, Pan and colleagues found that STEAP1 overexpression promotes ROS-mediated hyperproliferation of thyroid epithelial cells (42).

ROS participate in oncogenic signaling and elevated ROS levels are a salient feature of aggressive cancers (17, 18). Disturbances in the delicate ROS balance can lead to protein misfolding, accumulation of dysfunctional proteins, and activation of cellular stress responses (36). In accordance, STEAP1 silencing provokes transcriptional and posttranscriptional adaptations of oxidative stress responses comprising the redox, chaperone, endopeptidase, and UPS. These observations are compatible with the hypothesis that STEAP1 is associated with an enhanced oxidative stress phenotype in Ewing tumors. Consistently, we found that STEAP1 positively correlates with cytoplasmic and mitochondrial ROS levels. As mitochondrial morphology remained unaffected, we suppose that mitochondrial ROS levels change concomitantly with cytoplasmic ROS levels upon STEAP1-silencing, a mechanism also seen in the context of NOX proteins ("ROS-cross-talk"; ref. 43). The role of STEAP1 in ROS modulation is supported by *in silico* predictions and crystallography of STEAP proteins defining them as heme-containing redox enzymes (5, 13). Less aggressive ROS are well known to interact with heme iron of heme-containing proteins (15). Here, a nonenzymatic 2-electron oxidation of heme generates ferryl-heme and an unstable free radical that may be released as more aggressive

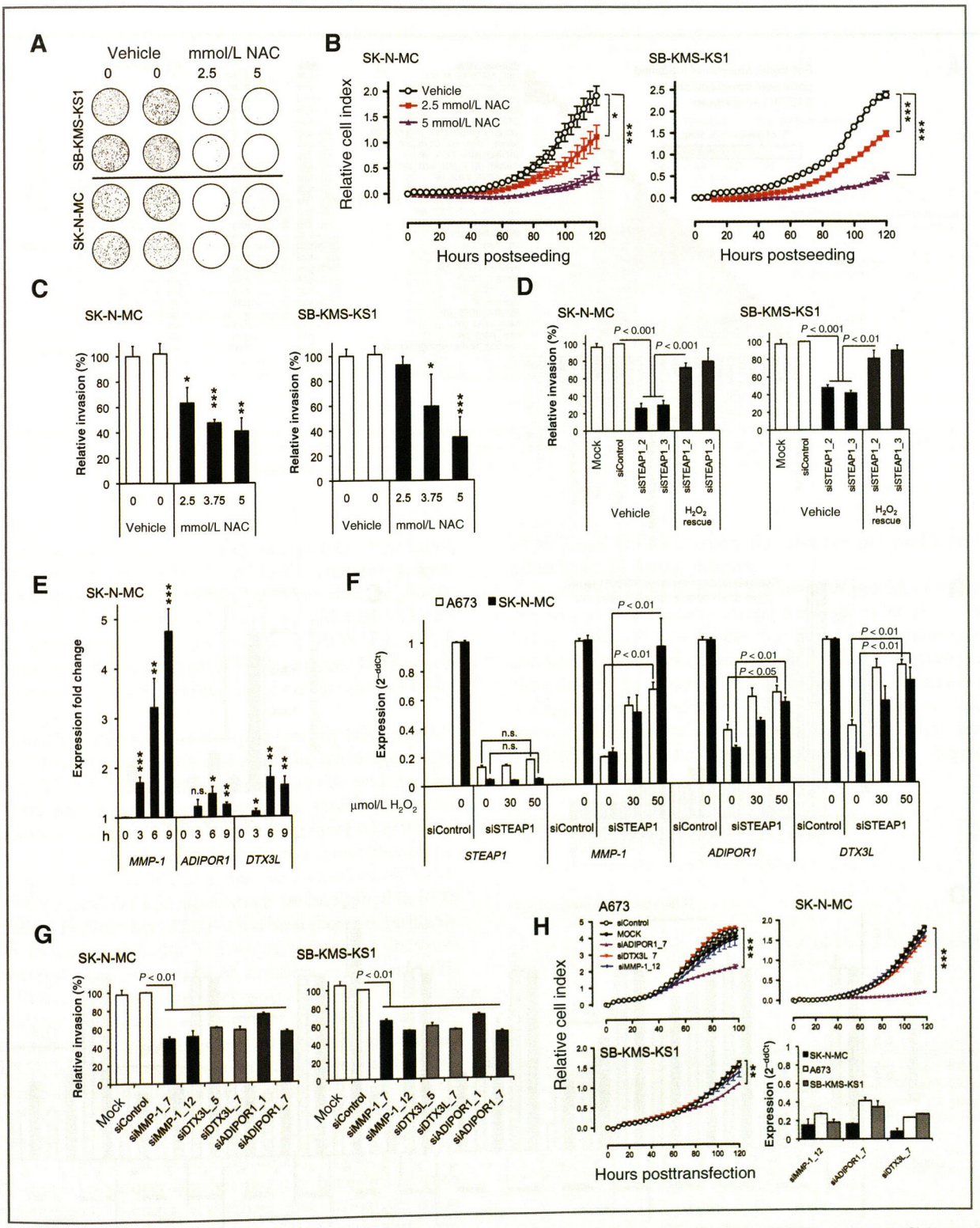

Figure 5. ROS are critical for Ewing tumor proliferation and invasiveness. A, colony formation of Ewing tumor cells treated with NAC or vehicle (H_2O). Images are representative for 3 experiments per cell line (duplicates/group). B, analysis of proliferation of SK-N-MC and SB-KMS-KS1 treated with NAC every 48 hours using xCELLigence. Mean ± SEM of 2 experiments per cell line (quadruplicates/group). C, analysis of invasiveness of SK-N-MC and SB-KMS-KS1 treated with NAC. Mean ± SEM of 2 experiments per cell line (pentaplicates/group). D, invasiveness of STEAP1-silenced SK-N-MC and SB-KMS-KS1 with/without H_2O_2 rescue. For H_2O_2 rescue, cells were treated periodically with H_2O_2 (cumulative dosage: 40 μmol/L). Mean ± SEM of 2 experiments per cell line (pentaplicates/group). E, MMP-1, ADIPOR1, and DTX3L expression in SK-N-MC treated with 50 μmol/L H_2O_2 for 0 to 9 hours. Mean ± SEM of 5 experiments (duplicates/group). F, analysis of STEAP1, MMP-1, ADIPOR1, and DTX3L expression in STEAP1-silenced A673 and SK-N-MC 6 hours after treatment with H_2O_2. Mean ± SEM of at least 2 experiments per cell line (duplicates/group). G, invasiveness of SK-N-MC and SB-KMS-KS1 transfected 48 hours before seeding. Mean ± SEM of 2 experiments per cell line (pentaplicates/group) H, analysis of proliferation of SK-N-MC and SB-KMS-KS1. Knockdown was confirmed by qRT-PCR (controls set as 1). Mean ± SEM of 2 experiments per cell line (heptaplicates/group). *, $P < 0.05$; **, $P < 0.01$; ***, $P < 0.001$; *t* test. n.s., nonsignificant.

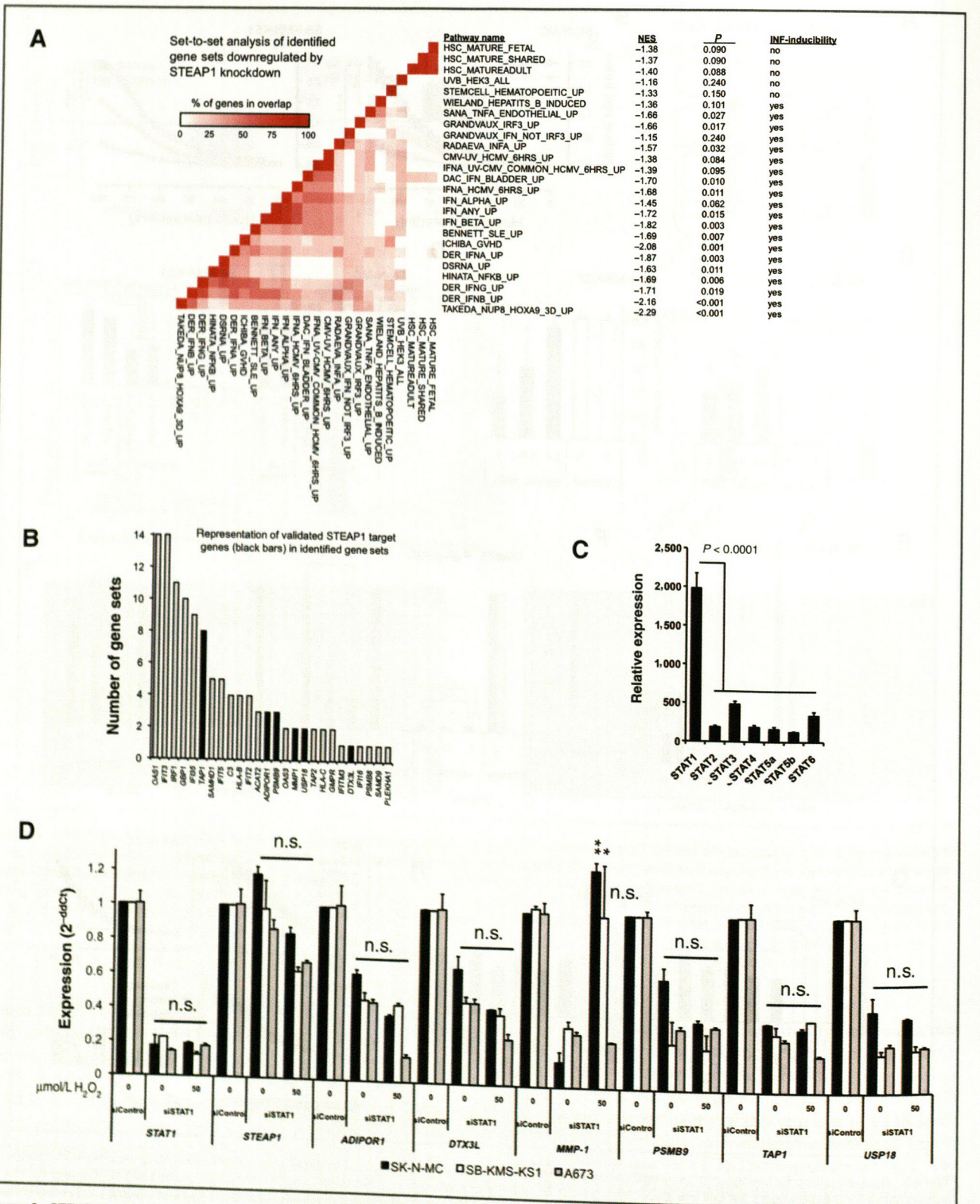

Figure 6. STEAP1 knockdown inhibits STAT1 activation. A, matrix diagram of the GSEA leading edge set-to-set analysis showing enrichment of IFN-related gene sets. NES, normalized enrichment score. B, gene-in-subset analysis reveals representation of validated STEAP1 target genes (black bars) within leading-edge genes. C, expression (mean ± SEM) of different STAT proteins in 26 Ewing tumor microarrays. D, expression analysis of STEAP1 target genes by qRT-PCR 48 hours after STAT1 silencing and H_2O_2 treatment (50 µmol/L for 6 hours).

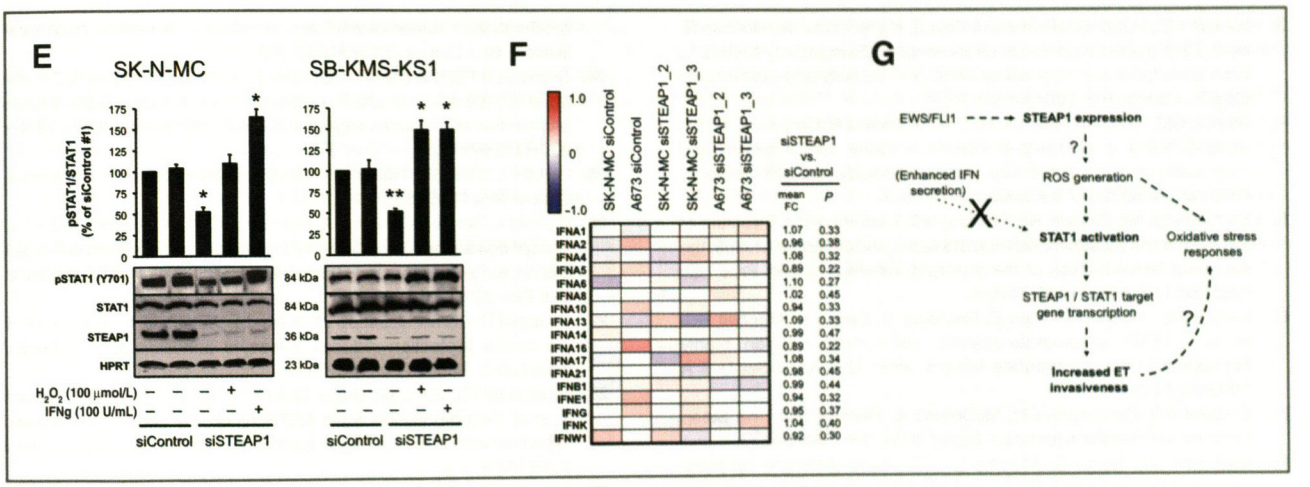

Figure 6. (*Continued*) E, Western blot and densitometric analysis of phospho-STAT1 (Y701) in Ewing tumor cells 48 hours after RNA interference and H_2O_2 (100 µmol/L) or IFN-γ (100 U/mL) stimulation (both 10 minutes). F, heatmap showing expression of IFN genes in Ewing tumor cells with/without STEAP1 silencing. G, simplified model of STEAP1-mediated target gene regulation. *, $P < 0.05$; **, $P < 0.01$; *t* test. FC, fold change; n.s., nonsignificant.

ROS in a site-specific manner depending on the localization of the protein (44, 45). As STEAP1 contains a ferric oxidoreductase, it is tempting to speculate that the protein generates ROS by itself (7, 42). However, although STEAP1 target genes appear to be downstream of ROS (Fig. 5F), it remains possible that part of STEAP1-induced ROS merely accompany upstream events involved in the STEAP1 phenotype.

Multiple studies proved that permanently elevated ROS levels activate prometastatic and proproliferative signaling in cancer (17, 19, 20). In agreement, we provide evidence that antioxidants reduce colony formation, proliferation, and invasion of Ewing tumor cells suggesting that Ewing tumors may benefit from an activated oxidative stress phenotype. Among STEAP1-regulated genes, we focused on *MMP-1*, *ADIPOR1*, and *DTX3L* all of which are implicated in ROS signaling. For instance, *MMP-1* has been shown to be highly ROS inducible (34, 46) and its overexpression increases invasiveness and metastasis of a variety of cancers (47). ADIPOR1 is the cognate receptor for adiponectin, which stimulates proliferation of hematopoietic stem cells (48). Although the precise function of the ubiquitin ligase DTX3L is not defined, recent work suggests that DTX3L monoubiquitylates histone H4 lysine 91 and thereby protects DNA from ROS (39). Here, we show that these genes are highly inducible by ROS and regulated by STAT1. STAT1 had been traditionally viewed as a mere IFN signal transducer but has recently been linked with aggressiveness, therapy resistance, and oxidative stress responses of several cancers (49, 50). Consistently, we prove that the coordinated expression of MMP-1, ADIPOR1, and DTX3L fosters the invasive and proliferative phenotype of Ewing tumors.

In summary, this work for the first time provides evidence that an activated oxidative stress phenotype enhances Ewing tumor malignancy: we show that STEAP1 overexpression promotes proliferation, invasiveness, anchorage-independent colony formation, tumorigenicity, and metastasis of Ewing tumors. Because STEAP1 is overexpressed in a wide variety of carcinomas, its oncogenic function may have general relevance for tumor progression and targeted therapy.

Disclosure of Potential Conflicts of Interest

No potential conflicts of interest were disclosed.

Acknowledgments

The authors thank Barbara Grunewald and Veit Buchholz for fruitful discussion and Ulrich Welsch for his help with electron microscopy.

Grant Support

This work was supported by the TU München (B08-05; A09-02), the Deutsche Forschungsgemeinschaft (GR3728/1.1, SFB/TR22, and EB740/6.1), the Wilhelm-Sander-Stiftung (2009.901.1), the Ministerium für Innovation, Wissenschaft und Technologie des Landes Nordrhein-Westfalen, the EU 7thFP Metoxia, the Bundesministerium für Bildung und Forschung (BMBF), and the Translational-Sarcoma-Research-Network supported by the BMBF (FK 01GM0870).

The costs of publication of this article were defrayed in part by the payment of page charges. This article must therefore be hereby marked *advertisement* in accordance with 18 U.S.C. Section 1734 solely to indicate this fact.

Received November 4, 2011; accepted November 7, 2011; published OnlineFirst November 11, 2011.

References

1. Burdach S, Jurgens H. High-dose chemoradiotherapy (HDC) in the Ewing family of tumors (EFT). Crit Rev Oncol Hematol 2002;41:169–89.

2. Delattre O, Zucman J, Melot T, Garau XS, Zucker JM, Lenoir GM, et al. The Ewing family of tumors–a subgroup of small-round-cell tumors defined by specific chimeric transcripts. N Engl J Med 1994;331:294–9.

3. Staege MS, Hutter C, Neumann I, Foja S, Hattenhorst UE, Hansen G, et al. DNA microarrays reveal relationship of Ewing family tumors to both endothelial and fetal neural crest-derived cells and define novel targets. Cancer Res 2004;64:8213–21.
4. Richter GH, Plehm S, Fasan A, Rössler S, Unland R, Bennani-Baiti IM, et al. EZH2 is a mediator of EWS/FLI1 driven tumor growth and metastasis blocking endothelial and neuro-ectodermal differentiation. Proc Natl Acad Sci U S A 2009;106:5324–9.
5. Sendamarai AK, Ohgami RS, Fleming MD, Lawrence CM. Structure of the membrane proximal oxidoreductase domain of human Steap3, the dominant ferrireductase of the erythroid transferrin cycle. Proc Natl Acad Sci U S A 2008;105:7410–5.
6. Hubert RS, Vivanco I, Chen E, Rastegar S, Leong K, Mitchell SC, et al. STEAP: a prostate-specific cell-surface antigen highly expressed in human prostate tumors. Proc Natl Acad Sci U S A 1999;96:14523–8.
7. Ohgami RS, Campagna DR, McDonald A, Fleming MD. The Steap proteins are metalloreductases. Blood 2006;108:1388–94.
8. Vaghjiani RJ, Talma S, Murphy CL. Six-transmembrane epithelial antigen of the prostate (STEAP1 and STEAP2)-differentially expressed by murine and human mesenchymal stem cells. Tissue Eng Part A 2009;15:2073–83.
9. Tirode F, Laud-Duval K, Prieur A, Delorme B, Charbord P, Delattre O. Mesenchymal stem cell features of Ewing tumors. Cancer Cell 2007; 11:421–9.
10. Valenti MT, Dalle Carbonare L, Donatelli L, Bertoldo F, Giovanazzi B, Caliari F, et al. STEAP mRNA detection in serum of patients with solid tumours. Cancer Lett 2009;273:122–6.
11. Cheung IY, Feng Y, Danis K, Shukla N, Meyers P, Ladanyi M, et al. Novel markers of subclinical disease for Ewing family tumors from gene expression profiling. Clin Cancer Res 2007;13: 6978–83.
12. Challita-Eid PM, Morrison K, Etessami S, An Z, Morrison KJ, Perez-Villar JJ, et al. Monoclonal antibodies to six-transmembrane epithelial antigen of the prostate-1 inhibit intercellular communication *in vitro* and growth of human tumor xenografts *in vivo*. Cancer Res 2007;67:5798–805.
13. Sanchez-Pulido L, Rojas AM, Valencia A, Martinez AC, Andrade MA. ACRATA: a novel electron transfer domain associated to apoptosis and cancer. BMC Cancer 2004;4:98.
14. von Rozycki T, Yen MR, Lende EE, Saier MH Jr. The YedZ family: possible heme binding proteins that can be fused to transporters and electron carriers. J Mol Microbiol Biotechnol 2004;8: 129–40.
15. Lambeth JD. NOX enzymes and the biology of reactive oxygen. Nat Rev Immunol 2004;4:181–9.
16. Ohgami RS, Campagna DR, Greer EL, Antiochos B, McDonald A, Chen J, et al. Identification of a ferrireductase required for efficient transferrin-dependent iron uptake in erythroid cells. Nat Genet 2005;37: 1264–9.
17. Szatrowski TP, Nathan CF. Production of large amounts of hydrogen peroxide by human tumor cells. Cancer Res 1991;51:794–8.
18. Grek CL, Tew KD. Redox metabolism and malignancy. Curr Opin Pharmacol 2010;10:362–8.
19. Smith DG, Magwere T, Burchill SA. Oxidative stress and therapeutic opportunities: focus on the Ewing's sarcoma family of tumors. Expert Rev Anticancer Ther 2011;11:229–49.
20. Luo J, Solimini NL, Elledge SJ. Principles of cancer therapy: oncogene and non-oncogene addiction. Cell 2009;136:823–37.
21. Klein A, Guhl E, Zollinger R, Tzeng YJ, Wessel R, Hummel M, et al. Gene expression profiling: cell cycle deregulation and aneuploidy do not cause breast cancer formation in WAP-SVT/t transgenic animals. J Mol Med (Berl) 2005;83:362–76.
22. Kobayashi H, Nagato T, Sato K, Aoki N, Kimura S, Murakami M, et al. Recognition of prostate and melanoma tumor cells by six-transmembrane epithelial antigen of prostate-specific helper T lymphocytes in a human leukocyte antigen class II-restricted manner. Cancer Res 2007;67:5498–504.
23. Grunewald TG, Kammerer U, Winkler C, Schindler D, Sickmann A, Honig A, et al. Overexpression of LASP-1 mediates migration and proliferation of human ovarian cancer cells and influences zyxin localisation. Br J Cancer 2007;96:296–305.
24. Grunewald TG, Kammerer U, Schulze E, Schindler D, Honig A, Zimmer M, et al. Silencing of LASP-1 influences zyxin localization, inhibits proliferation and reduces migration in breast cancer cells. Exp Cell Res 2006;312:974–82.
25. Helson L, Das SK, Hajdu SI. Human neuroblastoma in nude mice. Cancer Res 1975;35:2594–9.
26. Diebold I, Djordjevic T, Petry A, Hatzelmann A, Tenor H, Hess J, et al. Phosphodiesterase 2 mediates redox-sensitive endothelial cell proliferation and angiogenesis by thrombin via Rac1 and NADPH oxidase 2. Circ Res 2009;104:1169–77.
27. Chappell D, Dorfler N, Jacob M, Rehm M, Welsch U, Conzen P, et al. Glycocalyx protection reduces leukocyte adhesion after ischemia/reperfusion. Shock 2009;34:133–9.
28. Grunewald TG, von Luettichau I, Welsch U, Dörr HG, Höpner F, Kovacs K, et al. First report of ectopic ACTH syndrome and PTHrP-induced hypercalcemia due to a hepatoblastoma in a child. Eur J Endocrinol 2010;162:813–8.
29. Lessnick SL, Dei Tos AP, Sorensen PH, Dileo P, Baker LH, Ferrari S, et al. Small round cell sarcomas. Semin Oncol 2009;36: 338–46.
30. Schmidt D, Harms D, Burdach S. Malignant peripheral neuroectodermal tumours of childhood and adolescence. Virchows Arch A Pathol Anat Histopathol 1985;406:351–65.
31. Baird K, Davis S, Antonescu CR, Harper UL, Walker RL, Chen Y, et al. Gene expression profiling of human sarcomas: insights into sarcoma biology. Cancer Res 2005;65:9226–35.
32. Acharya A, Das I, Chandhok D, Saha T. Redox regulation in cancer: a double-edged sword with therapeutic potential. Oxid Med Cell Longev 2010;3:23–34.
33. Landriscina M, Maddalena F, Laudiero G, Esposito F. Adaptation to oxidative stress, chemoresistance, and cell survival. Antioxid Redox Signal 2009;11:2701–16.
34. Nelson KK, Ranganathan AC, Mansouri J, Rodriguez AM, Providence KM, Rutter JL, et al. Elevated sod2 activity augments matrix metalloproteinase expression: evidence for the involvement of endogenous hydrogen peroxide in regulating metastasis. Clin Cancer Res 2003; 9:424–32.
35. Buchberger A, Bukau B, Sommer T. Protein quality control in the cytosol and the endoplasmic reticulum: brothers in arms. Mol Cell 2010;40:238–52.
36. Gorlach A, Klappa P, Kietzmann T. The endoplasmic reticulum: folding, calcium homeostasis, signaling, and redox control. Antioxid Redox Signal 2006;8:1391–418.
37. Seifert U, Bialy LP, Ebstein F, Bech-Otschir D, Voigt A, Schröter F, et al. Immunoproteasomes preserve protein homeostasis upon interferon-induced oxidative stress. Cell 2010;142:613–24.
38. Iwabu M, Yamauchi T, Okada-Iwabu M, Sato K, Nakagawa T, Funata M, et al. Adiponectin and AdipoR1 regulate PGC-1alpha and mitochondria by Ca(2+) and AMPK/SIRT1. Nature 2010; 464:1313–9.
39. Yan Q, Dutt S, Xu R, Graves K, Juszczynski P, Manis JP, et al. BBAP monoubiquitylates histone H4 at lysine 91 and selectively modulates the DNA damage response. Mol Cell 2009;36: 110–20.
40. Honda K, Takaoka A, Taniguchi T. Type I interferon [corrected] gene induction by the interferon regulatory factor family of transcription factors. Immunity 2006;25:349–60.
41. Simon AR, Rai U, Fanburg BL, Cochran BH. Activation of the JAK-STAT pathway by reactive oxygen species. Am J Physiol 1998;275: C1640–52.
42. Pan YZ, Li Y, Guo LR, Zhao YY, Zhao XJ. [Influence of expression of six transmembrane epithelial antigen of the prostate-1 on intracellular reactive oxygen species level and cell growth: an *in vitro* experiment]. Zhonghua Yi Xue Za Zhi 2008;88:641–4.
43. Daiber A. Redox signaling (cross-talk) from and to mitochondria involves mitochondrial pores and reactive oxygen species. Biochim Biophys Acta 2010;1797:897–906.

44. Galaris D, Skiada V, Barbouti A. Redox signaling and cancer: the role of "labile" iron. Cancer Lett 2008;266:21–9.
45. Chevion M. A site-specific mechanism for free radical induced biological damage: the essential role of redox-active transition metals. Free Radic Biol Med 1988;5:27–37.
46. Grange L, Nguyen MV, Lardy B, Derouazi M, Campion Y, Trocme C, et al. NAD(P)H oxidase activity of Nox4 in chondrocytes is both inducible and involved in collagenase expression. Antioxid Redox Signal 2006;8:1485–96.
47. Johansson N, Ahonen M, Kahari VM. Matrix metalloproteinases in tumor invasion. Cell Mol Life Sci 2000;57:5–15.
48. DiMascio L, Voermans C, Uqoezwa M, Duncan A, Lu D, Wu J, et al. Identification of adiponectin as a novel hemopoietic stem cell growth factor. J Immunol 2007;178:3511–20.
49. Khodarev NN, Minn AJ, Efimova EV, Darga TE, Labay E, Beckett M, et al. Signal transducer and activator of transcription 1 regulates both cytotoxic and prosurvival functions in tumor cells. Cancer Res 2007;67:9214–20.
50. Schultz J, Koczan D, Schmitz U, Ibrahim SM, Pilch D, Landsberg J, et al. Tumor-promoting role of signal transducer and activator of transcription (Stat)1 in late-stage melanoma growth. Clin Exp Metastasis 2010;27:133–40.